BER the international journal of bridge engineering management and research

Precision Assessment of Reinforced Concrete RC Bridge Pier Resilience under High-Velocity Vehicle Impact Using an Energy-Based Analytical Model

Suman Roy*

Submitted: 22 May 2025 **Accepted:** 20 June 2025 **Publication date:** 10 July 2025

DOI: 10.70465/ber.v2i3.40

Abstract: The structural reliability of bridge piers under dynamic loading is a key factor in ensuring infrastructure resilience, particularly in the face of high-speed vehicular impacts. While often considered less critical than seismic or blast events, such impacts can significantly compromise pier capacity, thereby increasing vulnerability in multi-hazard scenarios. Existing design codes provide well-established criteria for seismic and blast resistance, but offer limited guidance for addressing high-velocity vehicle impacts, highlighting a critical gap in current engineering practice. This study addresses that gap by investigating the energy dissipation behavior of reinforced concrete piers subjected to high-speed impacts, employing a spring-action model that explicitly includes the contribution of concrete—an aspect frequently overlooked in conventional modeling approaches. Comparative simulations are conducted with and without the concrete's energy-absorbing effects to evaluate its role in post-impact structural performance. Monte Carlo simulations are used to assess failure probabilities and quantify post-impact energy dissipation, supported by uncertainty analysis revealing up to a maximum 33% variation stemming from modeling assumptions. The findings underscore the significant role of concrete in absorbing impact energy, improving damage prediction, and enhancing overall structural reliability. This research offers valuable insights to guide the development of advanced design methodologies and support the refinement of code provisions, ultimately promoting more resilient and efficient bridge pier systems capable of withstanding short-duration, high strain-rate loading events.

Author keywords: High-velocity truck impact; RC prototype bridge pier; depiction of failure zone; resilience of pier due to concrete contribution; Monte Carlo (MC) simulations; confidence interval of failure; and uncertainty assessment of normalized limit state equation (LSE)

Introduction

As transportation infrastructure faces growing exposure to high-velocity vehicular impacts—driven by increased traffic volumes, higher vehicle speeds, and evolving threat scenarios—a significant gap has emerged in structural design practice. While current codes offer well-established guidelines for resisting seismic and blast loads, grounded in decades of research and embedded within performance-based frameworks, they provide limited and often simplistic treatment of vehicle-induced impact loads, particularly on critical elements such as reinforced concrete (RC) bridge piers. Unlike earthquakes and blasts, whose dynamic effects are well understood and standardized,[1] vehicular collisions remain insufficiently addressed, leaving bridges susceptible to localized failures or even progressive collapse, especially when subjected to short-duration, high strain-rate loading. To address this deficiency, it is imperative to develop refined assessment tools and design methodologies that accurately capture the distinctive features of vehicular impacts, including short-duration dynamic load application, nonlinear energy dissipation, and material degradation under extreme strain rates. This analytical study contributes to that effort by simulating the dynamic response of RC bridge piers across a range of impact scenarios, from quasi-static to fully plastic conditions, to evaluate their post-impact performance and failure modes. Given the exposed positioning and geometric vulnerability of bridge piers to diverse dynamic actions such as seismic events, blast loads, and vehicular collisions, a comprehensive understanding of their behavior under such complex loading is essential for advancing the resilience and safety of modern bridge systems. While the behavior of RC bridge piers under seismic and blast loads has been widely studied, the response of these piers to vehicular impacts—ranging from low to high intensity—has not received comparable attention. This is despite the fact that vehicle impacts occur more frequently than both seismic and blast events, highlighting a significant gap in

*Corresponding Author: Suman Roy. Email: roy.suman@usu.edu, sumanroy74@gmail.com

Department of Civil and Environmental Engineering, Utah State University, Logan, USA

Discussion period open till six months from the publication date. Please submit separate discussion for each individual paper. This paper is a part of the Vol. 2 of the International Journal of Bridge Engineering, Management and Research (© BER), ISSN 3065-0569.

the current body of research.[2] A growing concern is that increased vulnerability to vehicle collisions, which may be exacerbated by factors such as driver negligence and the exposed nature of RC bridge piers, can lead to catastrophic structural failures. Such failures could result in the collapse of the entire bridge. In less severe cases, localized damage such as cracking can occur, which, if left unaddressed, may lead to functional impairments that render the pier non-serviceable. Investigations into the serviceability and age of existing bridge structures suggest that many RC bridges, particularly those subjected to high-intensity or multi-hazard loading events, are at risk of significant degradation. These events can cause permanent deformation and irreversible damage, further compromising the integrity of the structure.

In light of these concerns, there is a pressing need to revisit and upgrade existing design methodologies to enhance the robustness of critical structural elements that must withstand such extreme load conditions. Present-day design codes typically focus on the application of individual hazardous load types, such as flexural, axial, shear, and torsional forces, each considered in isolation. Previous studies have typically assumed no contribution from concrete in resisting vehicular impacts, resulting in overly conservative models that may underestimate the structural capacity and hinder opportunities for design optimization. Furthermore, the influence of high strain-rate loading conditions, such as those generated by vehicular impacts, is not sufficiently addressed in current codes.[3,4] This article compares the function of concrete with the comparatively conservative approach of considering no contribution from concrete during vehicle impact. Unfortunately, research on multi-hazard scenarios, especially those involving dynamic vehicle impacts, has been limited, leaving a gap in the understanding of how these events interact and contribute to the overall failure of bridge piers. Although studies have been conducted on sequential loading from blast and vehicular impacts, the focus has generally been on the post-performance behavior of piers at the collapse stage rather than on predictive models for multi-hazard interactions.[4,5]

To ensure satisfactory structural performance, RC bridge piers must exhibit ductile behavior when subjected to short-duration dynamic loads. Ductility allows the structure to deform under high loads without experiencing catastrophic failure, thereby providing crucial energy dissipation during the impact event.[6] Several dynamic analysis methods have been proposed to characterize the strength, deformability, and energy absorption characteristics of RC bridge piers under dynamic loading. A flexure-dominated approach to analyzing these factors, with an emphasis on energy dissipation, is presented in reference.[7] However, prior research in this area has typically been conservative, often neglecting the contributions of the concrete itself during impact events. In contrast, the present study takes a more comprehensive approach by evaluating both the conventional conservative method (which assumes no contribution from concrete) and a more holistic approach, considering the concrete's role in energy absorption, recoil, and spring action during vehicle impacts.

In an effort to create a more accurate and reliable model, this study develops a method that accounts for all potential energy parameters involved in short-duration impacts. This includes the assessment of the aspect ratio and its function in dissipating energy during impact events. Limit state equations (LSEs) are formulated to incorporate all relevant energy parameters, allowing for a more robust prediction of failure probabilities and the corresponding reliability of RC bridge piers with high concrete compressive strengths.[8] The vehicle specifications used in the study are based on data from[9] and the time of impact is treated as a nondeterministic variable to account for the inherent uncertainty in real-world scenarios. Monte Carlo (MC) simulations were employed to generate a large dataset; more than 11,000 data points for each case have been utilized to assess the reliability of the pier under varying domains of energy dissipation conditions.

The primary objective of this study is to evaluate the effects of vehicular impact on the structural reliability of circular RC bridge piers. This evaluation is carried out through the lens of LSEs governed by energy dissipation principles. The study also takes a comprehensive approach by assessing the confidence levels, uncertainties, and risks associated with potential failure scenarios. By analyzing the interaction between various load types, this research aims to provide valuable insights into the structural integrity of RC piers under dynamic impact conditions. The results show strong agreement with theoretical predictions, confirming that the proposed model is both accurate and reliable. Consequently, this model can be confidently used for both design and risk assessment purposes, contributing to safer and more resilient bridge infrastructure.

Precisely, the study bridges a significant gap in the existing literature by not only examining the effects of vehicular impacts on RC bridge piers but also by developing a more nuanced and robust approach to predicting the structural behavior under multi-hazard scenarios. With its focus on energy dissipation, reliability, and the interaction between various loading events, the findings from this research are crucial for improving the safety, design, and resilience of RC bridge piers subjected to dynamic loads.

Methodologies

This study employs a representative RC bridge pier as the primary test specimen to showcase the effectiveness and robustness of the proposed methodology for assessing structural integrity and performance. The pier is designed with an unsupported length of 8 ft 6 inches (2.59 m), which serves as a critical factor for evaluating the behavior of the structure under various loading conditions. Notably, both ends of the pier are restrained to prevent any yielding, rotation, or distortion at the support points. This means the boundary conditions of the pier are considered as both ends being restrained from displacement in any direction and from rotation at the top and bottom, as shown in Fig. 1. This setup is essential for simulating real-world conditions where bridge piers must maintain their integrity and resist

deformation, even when subjected to external forces. The choice of a circular cross-section for the pier, with an external diameter of 21 inches (53.34 cm), contributes to a uniform distribution of stress along its length, improving the overall performance and durability of the pier under loads.

The longitudinal reinforcement in this pier is a key design feature, providing essential tensile strength to resist typical forces experienced by bridge components. It consists of six #8 steel bars made from ASTM A706 Grade 60 steel, which is a specification set by the American Society for Testing and Materials (ASTMs). ASTM standards ensure that the steel meets strict requirements for chemical composition, mechanical properties, and performance, making it suitable for critical structural applications. Grade 60 indicates a minimum yield strength of 60 ksi (413.68 MPa), combined with excellent ductility, enabling the pier to sustain significant deformation without failure. The reinforcement bars run continuously from the top of the pier down to its foundation and are strategically arranged to maximize the pier's structural capacity while promoting efficient use of materials and facilitating construction. Together, these bars enhance the pier's resistance to bending moments and axial loads, ensuring reliable performance as a resilient component within the bridge structure.

In addition to the longitudinal reinforcement, the shear resistance of the pier is addressed through the use of #4 steel bars arranged at 2.5-inch (63.5 mm) on-center spacing. These shear reinforcement bars are designed to prevent shear failure, which is often the weak point in concrete structures subjected to lateral loads or seismic forces. The shear reinforcement is arranged in a spiral pattern, which is particularly effective in distributing shear stresses evenly throughout the pier, thus minimizing the risk of localized failure. Moreover, the transverse steel ratio (ρ_t) is maintained at 0.06%, which adheres to the minimum requirements set by the American Concrete Institute (ACI) in their 2011 standards. This ensures that the pier has an adequate level of shear reinforcement, in compliance with industry best practices and safety standards.

The consistent vertical pitch of the shear reinforcement at 2.5 inches (63.5 mm) further contributes to the stability and resilience of the pier, ensuring that the distribution of shear resistance remains uniform along the entire length of the pier. This attention to detail in the design of the shear reinforcement is crucial for preventing any potential weak points that could compromise the pier's overall performance, especially under extreme loading conditions. By adhering to the minimum requirements outlined in the ACI 2011 standards,[1] the design ensures that the pier will not only meet the necessary safety factors but also exhibit improved durability and serviceability throughout its lifespan. The shear reinforcement's uniformity also plays a significant role in mitigating the risk of cracking, which could otherwise lead to structural degradation over time. The prototype RC pier, complete with its detailed end conditions and cross-sectional configuration, is visually represented in Fig. 1, providing a comprehensive illustration of the specimen used in the study. This visual aid helps to clarify the design choices and structural elements incorporated into the pier, making it easier for researchers and engineers to understand the significance of each component and ensuring precise engineering in enhancing the safety, longevity, and performance of critical infrastructure components such as bridge piers.

Using these dimensions, the aspect ratio (L/h) of the pier is calculated as 4.85. The gross cross-sectional area of the pier (A_g) is 346.5 in^2 (2235.48 cm^2), and the total area of the cross-section of steel (A_s) is 4.74 in^2 (30.58 cm^2). The steel ratio is calculated as ($\rho_l = A_s/A_g$) 0.01368. The nominal axial load $P_{N,Design}$ of the pier is computed to be 687.50 kips (3058.15 kN). Using these dimensions, a mathematical model is developed by modifying equations from the literature and journals[8] to evaluate the geometries and design parameters of the representative pier.

This research presents a performance-based damage assessment methodology for RC bridge piers subjected to vehicular impact. On impact from a vehicle, RC piers sustain different levels of damage depending on the geometry, material properties, and boundary conditions of the pier, as well as the mass, velocity, and type of vehicle. Damage incurred by the pier also depends on the impact duration and, therefore, the maximum dynamic impact shock (I_{dyn}) transmitted into the RC pier. The severity of damage to the pier depends on these factors and influences the decisions to be made regarding further use of the pier. Some piers sustain little damage and may be retrofitted and strengthened for continued service, while others, which suffer more extensive damage, would require immediate replacement should the bridge be kept in service. However, in post-impact inspections to quantify the damage to the pier, it might be impossible to accurately estimate the speed of the impacting vehicle. Therefore, the practical method to determine post-impact lateral deformation (Δ) and the effective stiffness (EI_{eff}) of the pier shall be an alternative method to be used as a field assessment by simple inspection methods.

The concept of maximum deflection (Δ_{max}) of the post-impacted RC pier, with both ends restrained, preventing displacement and rotation in all directions, under a concentrated and compressive load, is used to relate the dynamic impact force (I_{dyn}), as shown in Fig. 1. It is also utilized as an alternative method for the computation of dynamic impact (I_{dyn}). This relationship is shown in Eq. (1).[9]

$$I_{dyn} = \frac{3EI_{eff}(3L - 2a)^2\Delta_{max}}{2a^2b^3} \tag{1}$$

where EI_{eff} is the effective stiffness (i.e., flexural rigidity) of the pier; L is the unrestrained length of the pier; a is the distance from the bottom of the pier to the point of impact; b is the distance from the upper end of the pier to the point of impact; and Δ_{max} is the maximum post-impact deflection occurring in the pier from the dynamic impact force (I_{dyn}).

Nearly all design codes emphasize the importance of incorporating the effective flexural rigidity (EI_{eff}). In light of this, some codes specifically call for the calculation of both initial and effective stiffness values. The initial effective stiffness, as commonly proposed, is typically defined as 0.5EcIg, where E_c represents the modulus of elasticity of concrete and I_g denotes the gross moment of inertia. This approximation is

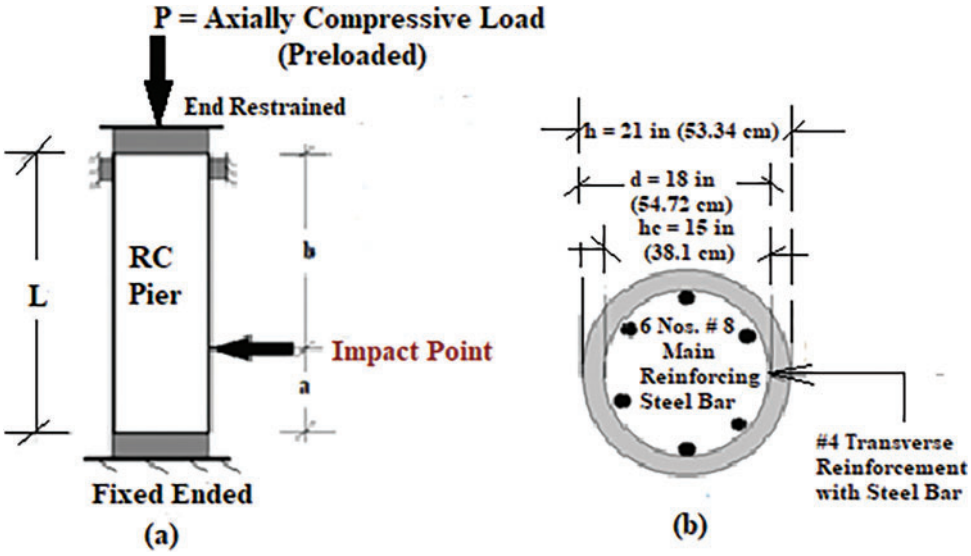

Figure 1. (a) Pier end conditions, and (b) pier cross-section

based on the well-established fact that the flexural rigidity of RC piers diminishes as lateral deflections and crack propagation increase.[10] However, the actual effective stiffness (EI_{eff}) is used in more precise computations of lateral deformations, as described by the relationship in Eq. (1).[9]

Energy dissipation mechanism

The energy dissipation mechanism between an impacting truck and a prototype RC bridge pier is a complex phenomenon that refers to how kinetic energy from the moving vehicle is absorbed, transformed, or redirected by the pier and its surrounding system during a collision. Understanding this mechanism is critical for designing crash-resistant bridge infrastructure. This comprises:

(a) Material deformation, including:
Concrete Crushing: Upon impact, localized crushing of concrete occurs at the contact region, converting kinetic energy into internal strain energy and heat.
Steel reinforcement yielding: The internal steel reinforcement bars (rebar) deform plastically, absorbing a significant portion of the energy. Yielding of steel is one of the most efficient mechanisms for energy absorption.

(b) Cracking and Spalling
Flexural cracking: If the impact induces bending, cracks form along the tension face of the pier, especially at the base. These cracks absorb energy as they propagate.
Shear cracking: At higher impact forces, diagonal shear cracks may develop, leading to further energy dissipation.
Concrete spalling: Layers of concrete may flake off (spall) under intense stress, especially at the point of impact. The energy used to fracture and eject this material contributes to overall dissipation

(c) Vibration and Wave Propagation
The impact generates stress waves that propagate through the structure. Part of the energy is transformed into vibrational energy, which may be damped over time or by the surrounding foundation system.

(d) Damage to the impacting vehicle
The vehicle itself absorbs some of the impact energy through crumpling and deformation. While not part of the pier's dissipation, it is relevant to the total energy balance in the system. In this study, post-dissipated energy due to the truck-impacted post behavior of the representative pier has been investigated.

Prediction of plastic hinge length (L_p) of dynamic impacted pier

For RC flexural members, the plastic (permanent) deformation is typically localized in a smaller zone after the yielding of the member. The performance of the plastic hinge zone is critical for flexural members, as it governs the load-carrying capacities of the member.[11] The overall energy dissipation capacity of the RC member can be evaluated by using the energy dissipated by the steel rebar, while the concrete contribution is not typically considered due to its relatively small ductility.[12] Reinforcing steel, being isotropic, dissipates high energy by exhibiting plastic behavior compared to concrete, which dissipates considerably less energy.[13] For that reason, the overall energy dissipation is considered by the flexural and tensile reinforcing bars. The maximum predicted plastic hinge length (L_p) has been previously defined and is shown in Eq. (2).[14]

$$L_p = 0.08 * L + 0.15 * f_y * d_b \quad (2)$$

where L_p and L are the lengths of the plastic hinge and the unsupported length of the pier, respectively; d_b is the bar diameter of the longitudinal steel reinforcement; and f_y is the

yield strength of the main reinforcing steel bar, considered as 60 ksi (413.685 MPa) for this study.

The plastic hinge length ratio (L_p/L) can be defined as ψ, and using this definition, after rearranging Eq. (2), yields Eqs. (3) and (4), respectively.

$$\psi = 0.08 + 9.0 * (d_b/h)/(L/h) \quad (3)$$

$$\psi = 0.08 + 9.0 * (\gamma/\eta) \quad (4)$$

where γ and η are used to replace the ratios d_b/h and L/h (aspect ratio), respectively.

This replacement will help determine ψ precisely using an analytical method that plays a pivotal role. The ratio ψ helps characterize how much of the element is experiencing plastic deformation relative to its total length. A higher ratio indicates a larger region of plastic deformation, typically associated with more inelastic behavior and greater potential for energy dissipation in short-duration, high strain-rate loading. In design, controlling this ratio can help prevent excessive damage to structures during extreme loading conditions.

Rate of plastic hinge formation considering strain rate ($\acute{\varepsilon}$) of reinforcing steel

A plastic hinge in a column refers to a localized zone where the structural element undergoes significant plastic deformation under loading, allowing it to rotate without a substantial increase in moment. This phenomenon occurs when the stress in the material reaches the yield strength, causing the section to behave plastically rather than elastically. In seismic and structural engineering, plastic hinges are critical because they represent regions where the column can dissipate energy through controlled deformation, enhancing the ductility and overall resilience of the structure. However, the formation and location of plastic hinges must be carefully considered in design to avoid premature failure or collapse, especially in RC columns, which are confined by providing lateral steel and main reinforcement details that influence hinge behavior. Properly designed plastic hinges allow structures to undergo large displacements while maintaining load-carrying capacity, thus providing important warning signs before failure. However, when enough plastic hinges form in a structure (typically equal to the degree of static indeterminacy + 1), the structure becomes a mechanism. This allows rotation to occur freely at those hinges, and the structure can no longer carry additional load, leading to collapse.

Plastic hinge formation in this research has been illustrated in terms of energy dissipation and the composite behavior of concrete and steel. Concrete is a nondeterministic, brittle material composed of aggregate and a cementitious matrix, and the reinforcing steel bar is an isotropic material exhibiting plastic and ductile behavior. Eq. (4) can be rewritten in terms of strain (ε) and modulus of elasticity (E_{st}) in the steel bar, yielding Eq. (5).

$$\psi = 0.08 + 0.15 * (E_{st} * \varepsilon) * (d_b/L) \quad (5)$$

where d_b expresses the diameter of the main reinforcing steel bars, considered as 1 in (25.4 mm) (#8 steel bar); L, indicating the unsupported length of the pier, is 8.5 ft (2.591 m); and E_{st}, the modulus of elasticity of steel, is taken as 29,000 ksi ($2*10^5$ MPa).

By taking the partial derivative of Eq. (5) with respect to time (t) and by inserting all values, Eq. (6) can be developed to incorporate.

$$\frac{\partial \psi}{\partial t} = 4.35 * 10^3 * (\acute{\varepsilon}) \quad (6)$$

where reinforcing steel strain rate is represented by $\acute{\varepsilon}$. This strain rate can therefore be evaluated as a function of the rate of formation of the plastic hinge length ratio ψ. This is represented in Fig. 2. Fig. 3 shows the comparative variations of steel strain rate with respect to plastic hinge length (L_p) and plastic hinge length ratio (ψ).

Evaluation of dissipation of energy (E_D)

RC members, irrespective of being vertical or horizontal, dissipate energy by experiencing inelastic behavior due to cyclic loading caused by the dynamic response incurred by high strain rate loading. In RC structures, the energy dissipation can be defined as the sum of the energy dissipated by both the concrete and steel. Concrete is a brittle material and hence less ductile. The evaluation of dissipated energy for a circular cross-section (e_D) RC pier for equivalent static behavior in car crash phenomena is as shown in Eq. (7).[14]

$$e_D = 4R_B * \rho * f_y \left(\frac{\pi h^3}{4}\right) \Phi_u * \left[(1-p)\left(\frac{h_s}{2h} - \frac{\varepsilon_y}{\Phi_d * h}\right) + p\left(0.5 - \frac{\varepsilon_y}{\Phi_{d*} h}\right)^2 \right] \quad (7)$$

'Bauschinger Effect', where e_D is the dissipated energy considered for the reinforcing steel bar, Φ_u is the maximum curvature; h is the overall diameter of the pier; h_s is the distance between the bar layers located between the boundaries; ε_y is the yield strain of the steel bar, considered as 0.0021; f_y is the yield stress of the steel bar (60 ksi); and p is the ratio of lateral steel ratio (ρ_t) to over longitudinal steel ratio (ρ_l), which can be calculated as $p = \rho_t/\rho_l = 0.0178/0.01368 = 1.28$. R_B represents the reduction factor comprising the 'Bauschinger Effect,' and is considered as 0.75.[15]

The maximum ultimate curvature, Φ_u, can be computed by using Eq. (8).[15]

$$\Phi_u = 2.45 * (\varepsilon_r/h) \quad (8)$$

where ε_r and h are already explained.

The main steel yield strain, ε_r is considered to be 0.06[15]; as such, Eq. (8) yields Φ_u as 0.007, which is a function of pier dimensions and geometries.

The yield curvature of the steel bar (Φ_y) can be determined using Eq. (9).[17,18]

$$\Phi_y = \alpha_{ST} * \left(\frac{\varepsilon_y}{h}\right) \quad (9)$$

where α_{ST} is the modification factor, considered as 2.12 for RC pier[15]; ε_y ($\varepsilon_y = f_y/E_{st}$) is the yield strain of steel, is computed as 0.00207, where E_s is modulus of elasticity of steel; and h has already been explained.[16]

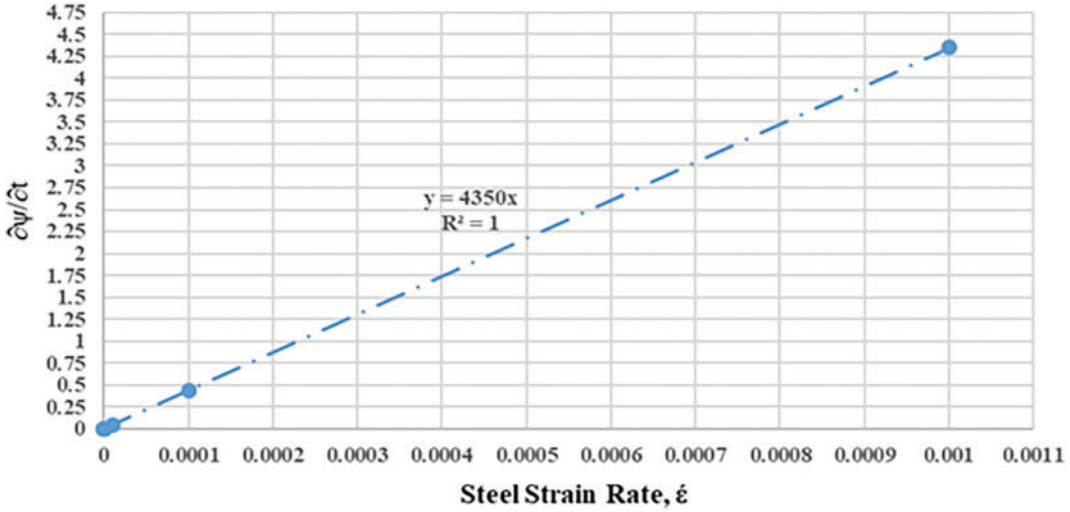

Figure 2. Steel strain rates with rate of formation of plastic hinge length ratio

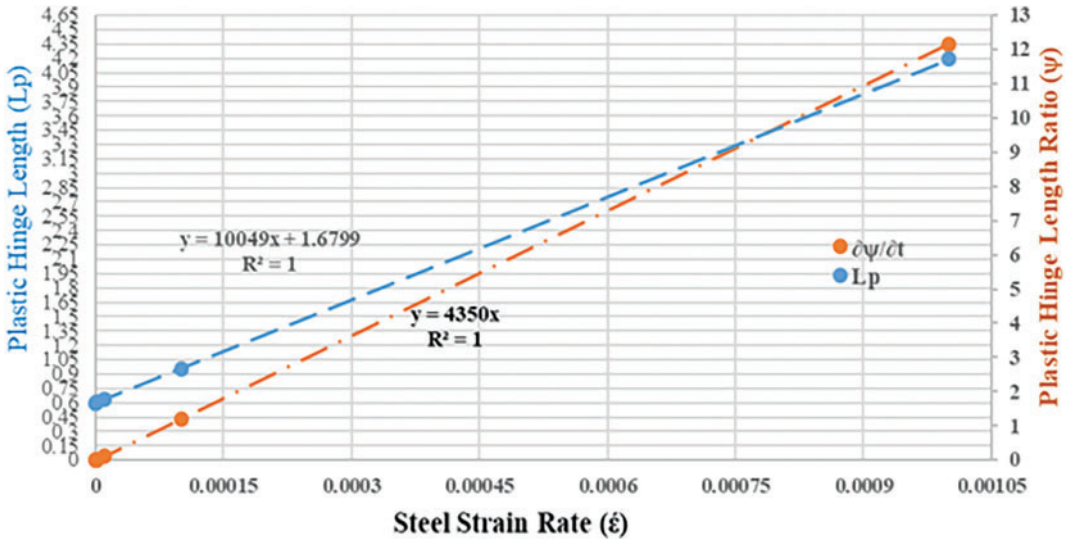

Figure 3. Steel strain rates with plastic hinge of plastic length ratio and plastic hinge length

Energy dissipation capacity based on kinematic behavior (e_{kh}) is a function of Φ_u and Φ_y, and is computed using Eq. (10).

$$e_{kh} = 4 * M_r * (\Phi_u - \Phi_y) \tag{10}$$

where M_r is the moment-carrying capacity of the circular pier cross-section (i.e., moment of resistance), which can be computed as shown in,[20] and Φ_u and Φ_y are already explained and shown to be determined.

The total energy to be dissipated at the plastic hinge as total energy, has been considered to be released during collapse and is computed from Eq. (11).[31]

$$E_D = e_D \tag{11}$$

For the representative pier, the moment carrying capacity (M_r) of the circular cross-section RC pier is computed as 6275.30 kip-in (709.013 kN-m) from Eq. (11). Using Eq. (11), Eq. (12) can be further rewritten as Eq. (12).

$$E_D = e_D * (L_p/L) * L = e_D * L * \psi \tag{12}$$

where $e_{D,}$ and L are already explained, and determining the ratio ψ (which is the ratio of the length of the plastic hinge over the total length of the pier specimen, i.e., $\psi = L_p/L$) can be determined using Eq. (13).

From Eq. (12), E_D can be expressed as shown in Eq. (13).

$$E_D = (e_D * L) * \left[0.008 + 0.15 * f_y * \left\{ \frac{d_b}{\left(\frac{L}{h}\right)} * h \right\} \right] \tag{13}$$

where E_D addresses the total energy dissipated during the formation of the plastic hinge caused by impact and has been illustrated in terms of $\frac{\gamma}{\eta}$ ratio, as shown in Fig. 3. Additionally, e_D, h, d_b, f_y, and L/h the aspect ratio have already been explained.

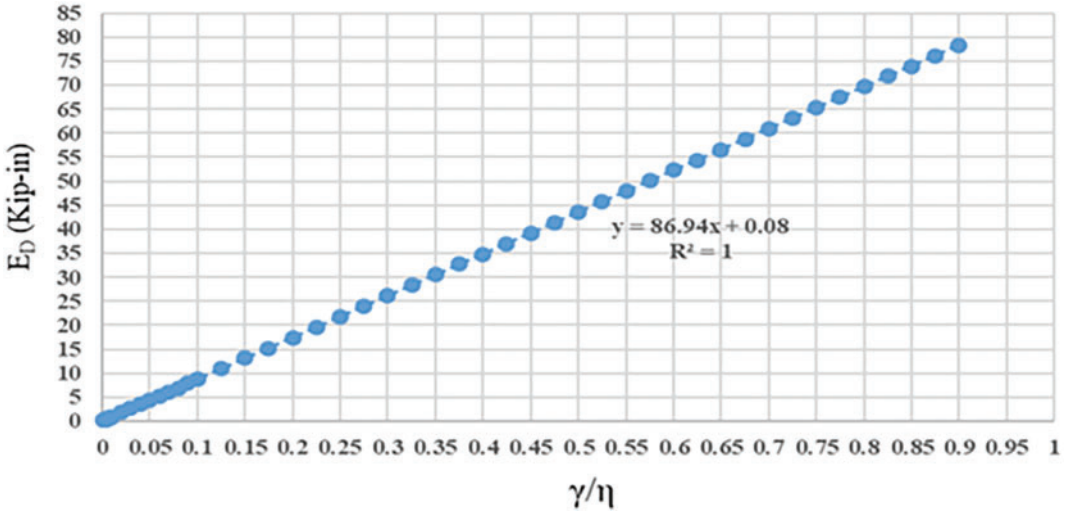

Figure 4. Total dissipated energy with bar diameter, pier diameter and aspect ratio

Fig. 3 shows a linear increment of E_D with the increment of $\frac{\gamma}{\eta}$, whereas Fig. 4 comprises shows a hyperbolic decrement of the aspect ratio (η) and a linear increment of $\frac{\gamma}{\eta}$ and E.

Using Eq. (13) and simplifying yields Eq. (14), which is a function of the aspect ratio (η) and pier dimension ratio (γ). Also, Fig. 4 includes a comparative estimate of E with η, comprising $\frac{\gamma}{\eta}$. As the $\frac{\gamma}{\eta}$ ratio is a governing function that includes pier geometry, it controls the energy dissipation as a post-impact effect.

$$E_D = 0.08 + 86.94 * \left(\frac{\gamma}{\eta}\right) \tag{14}$$

where $\frac{\gamma}{\eta}$ has been explained above.

In Eq. (14), $\gamma = d_b/h = 0.048$ and the aspect ratio, η = L/h, which has already been determined as 4.86.

Estimation of energy during vehicle impact

In this research, a displacement-based approach has been adopted considering the flexural response to high-velocity vehicle impact. The shear criterion considers that the pier might suffer brittle damage, localized spalling followed by shear failure, and deflection.[16,19] Vehicle data have been taken from published journals.[9] When a heavy mass vehicle moving at high velocity impacts an RC bridge pier, the pier may undergo localized shear deformations at any point in time.[20,21] In this study, kinetic energy of the moving vehicle before impact, the crushing energy causing recoiling of the frontal vehicle material, the post-impact potential energy of the RC pier, the spring action of the concrete pier, and the dissipation of energy due to impact are considered.

Crush energy

Crush energy refers to the amount of energy absorbed by a vehicle's structure during a collision as it deforms (or "crushes"). This energy is a critical factor in vehicle impact dynamics and plays a pivotal role in determining the severity of a collision and the forces transmitted to structures like bridge piers. The crush energy of a vehicle can be described as the amount of kinetic energy required to recoil the frontal part of the vehicle. This value depends on the frontal stiffness of the vehicle. Crush energy (U_{veh}) is given in Eq. (15).[16,19]

$$U_{veh} = \frac{1}{2}(F_{max} * u_0) \tag{15}$$

where F_{max} is the maximum forced inserted by the vehicle on pier during impact, and u_o is the recoiling velocity of the vehicle after impact.

In Eq. (15), u_o can be determined from using Eq. (16).

$$u_o = F_{max}/k \tag{16}$$

where k is the vehicular frontal stiffness, considered as 1.028 kip/feet (1500 kN/m), and F_{max} has been already addressed.

Combining Eqs. (15) and (16) yields Eq. (17).[19]

$$U_{veh} = \frac{1}{2}\left(\frac{F_{max}^2}{k}\right) \tag{17}$$

where U_{veh}, F_{max}, and k have already been explained.

Maximum vehicular force (F_{max}) has been formulated and can be estimated using Eq. (18).[32,33]

$$F_{max} = M_{veh} * V_{max}/t \tag{18}$$

where F_{max}, M_{veh}, V_{max}, and t have already been explained.

In Eq. (18), M_{veh} is the weight of the moving vehicle (42.11 kips or 187.32 kN for a semi-trailer as the maximum load, and 26.02 kips or 115.72 kN for the most frequently occurring vehicle load), V_{max} is the maximum velocity of the moving vehicle before impact (44.62 ft/s or 13.6 m/s for the maximum case, and 31.8 ft/s or 9.7 m/s for the most frequently occurring case), and t (time for impact) is the impact duration, considered as 10^{-3} to 10^{-4} s, which governs the strain rates of the steel rebar. In this study, the maximum case has been considered for maximum mass and maximum

velocity, whereas the most frequently occurring case has been taken as the most occurring mass with velocity.[20] Eq. (18) yields maximum inserted forces of 1878.95/t kips/s and 827.3/t kips/s for the extreme and most frequently occurring cases, respectively.

Potential energy of the pier

Potential energy of the pier (U_{col}) is the energy stored by the pier itself due to the contribution of steel and concrete. In this research, each case (i.e., the most vulnerable and the most frequently occurring) is fragmented into two individual cases. First, the concrete contribution is considered as spring action to recoil; and secondly, in a more conservative way, without considering the concrete spring action (recoiling action). The potential energy stored in the RC pier is quantified in Eq. (19).[19]

$$U_{col} = \int_0^{\delta max} F(\delta).d\delta \tag{19}$$

where F is represented as the resisting force inserted by the pier, and δ represents the deformation after impact, which is the average displacement of the pier [δ = (1.34 in. + 0.05 in.)/2 = 0.695 in. (17.653 mm)].

Spring action of the pier

To determine the energy responsible for providing the adequate stiffness (E_s) of the RC pier, the shear stiffness has been computed.[23] The pier stiffness has been considered to provide resistance against the shear experienced from horizontal dynamic impact. In this research, the pier displacement concept has been adopted to account for the displacement due to rebar slip in flexural deformations.[22] The energy evolved due to pier spring action (E_s) is introduced in Eq. (19) and as depicted in Fig. 6.[20]

$$E_s = 0.5 * k_{col} * \Delta^2 \tag{20}$$

where k_{col} and Δ represent pier stiffness and total deformation after recoiling.

In Eq. (19), the pier stiffness (k_{col}) can be computed from Eq. (21).[20]

$$k_{col} = 0.8 * E_c * I_g \tag{21}$$

where E_c is the modulus of elasticity of concrete (12247.45 ksi, calculated for 6 ksi compressive strength of concrete), and I_g is the gross moment of inertia of the pier section.

Computation of k_{col} using Eq. (20) yields $9.357 * 10^7$ kip/in pier stiffness while considering the concrete contribution in the RC pier against impact.

The pier resisting displacement (Δ) can be computed by considering the sum of the flexural ($\Delta_{flexure}$) displacement and shear (Δ_{shear}) displacement, and is shown in Eq. (22).[16]

$$\Delta = \Delta_{flexure} + \Delta_{shear} \tag{22}$$

where $\Delta_{flexure}$ and Δ_{shear} represent deformations due to bending and shear, respectively.

Eq. (23) provides the determination of $\Delta_{flexure}$.[16]

$$\Delta_{flexure} = \Phi_y * (L + L_{sp})^2/6 \tag{23}$$

where Φ_y is the strain rate of steel at first yield (0.00021), L is the total pier specimen length, and L_{sp} is the strain penetration length over which steel strain from the bar embeds into the concrete, transferring force via the bond between reinforcing steel and concrete. This can be evaluated from Eq. (24).

$$L_{sp} = 0.15 * f_y * d_b \tag{24}$$

where f_y and d_b are explained. L_{sp} represents strain penetration length.

After computation, Eq. (23) yields L_{sp} as 9.0 in. (228.6 mm). Furthermore, from Eq. (23), $\Delta_{flexure}$ is computed as 0.05 in. (1.27 mm).

Shear displacement (Δ_{shear}) is given in Eq. (25).[16]

$$\Delta_{shear} = \sum_{i=1}^{n} (r_{xy}^i + r_{xy}^{i+1})/(2 * h_i) \tag{25}$$

where r_{xy}^i and r_{xy}^{i+1} are the shear strains of the lower and upper sections of the ith segment, and h_i is considered as the height of each segment (Fig. 6).

The shear strain is calculated from Eq. (26),

$$r_{xy} = \tau_f / G \tag{26}$$

where τ_f is the shear stress and can be computed from Eq. (27), and G is the shear modulus (3×10^3 ksi) (20.7×10^3 MPa).[16] Eq. (26) yields r_{xy} as 6.043.

$$\tau_f = M/(h * d_f * L) \tag{27}$$

where M is the external maximum moment applied at the base [F_{max} * (3 ft) = $2.33 * 10^8$ kip-in.) (as shown in Fig. 5)] and hence computed as 2.33×10^8 kip-in (2.633×10^7 kN-m); h is the diameter of the pier; d_f represents the end-to-end distance of the longitudinal bar (18 in or 45.72 cm); and L is the pier length as discussed already.

Computing Eq. (27), τ_f has been determined as 6042.95 ksi (41.7×10^3 MPa).

Combining Eqs. (26) and (27) yields Δ_{shear} as 217.55 in. (552.58 cm). The combination of Eqs. (19)–(26) results in E_s as 2.12×10^{12} kip-in. (2.4×10^{11} kN-m).

Prediction of limit state equation for energy concept

Limit state equations (LSEs) incorporating failure prediction using energy (E) analyses have been developed in this research. Analytical models depicting LSE to assess failure during dynamic impact have been determined for a representative pier. Different dynamic cases are considered for intensive assessment. Time (t) during impact for quasi-static to plastic deformation is considered as 10^{-3}–10^{-4} s, hence considered as nondeterministic for short-duration impact and high strain rate loading. For that, the mean (μ) and coefficient of variation (V) considered in this research are 0.00055 and 0.1, respectively.[4] Thus, the standard deviation (σ) has been computed as 0.000055 ($\sigma = \mu \times V$), and time for dynamic impact is considered as normally distributed. Steel strain rates are considered to evolve numerical modeling. Finally, MC simulations predicting individual cases are carried out for 11000 data points to predict failure (statistical parameters mean and standard deviation converged at about

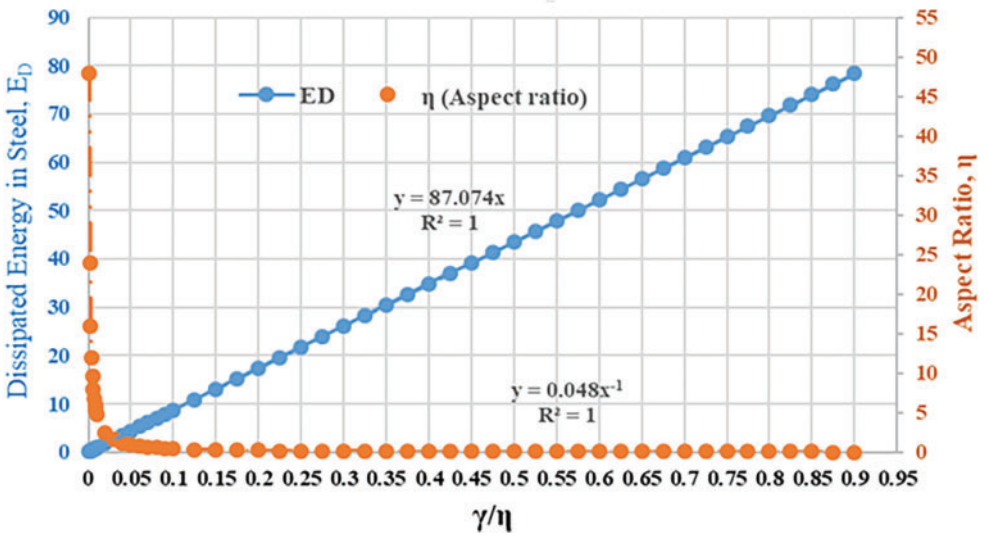

Figure 5. Comparison of dissipated energy and aspect ratio

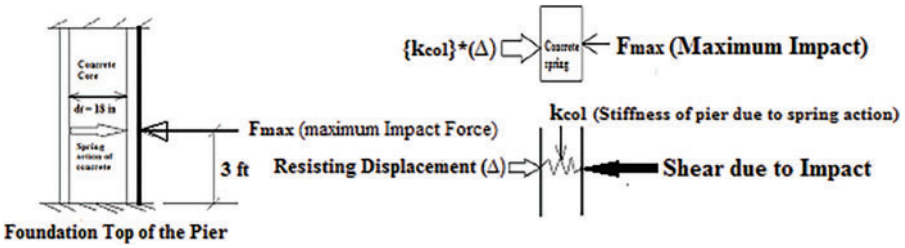

Figure 6. Concrete spring action and equivalent spring model

this number of simulations) and to determine reliability indices (β) from the respective probabilities of failure (P_f) resulting from MC simulations, considering concrete contribution as a spring effect, and the conservative approach without concrete contribution as spring action as shown in Fig. 6.

Without consideration of concrete contribution

The probability of failure, P_f, is considered to be highest when the system's energy condition reaches the critical threshold, specifically when the elastic modulus E becomes zero or negative. This condition is illustrated in Eq. (28), where the kinetic energy of the vehicle involved in the impact must not exceed the sum of the following:

- due to various types, frequent, and most frequent occurrences of vehicle crashes to RC bridge piers due to their exposed face at the roadside.
- the potential energy stored in the RC pier specimen,
- the amount of strain energy dissipated due to impact forces,
- the energy associated with the recoil of the vehicle's frontal materials, and
- the spring energy generated by the deformation of the sacrificial layer and core concrete.

While this conservative analysis approach provides a higher safety margin, simulations have been conducted excluding the spring action of the concrete. However, when spring action is considered, the results are more aligned with practical and real-world scenarios, offering a more accurate estimation of P_f as shown in Eq. (28). These simulations, which incorporate spring action, tend to provide a better approximation of the actual system's behavior under impact, highlighting the importance of considering such dynamic effects for more reliable and realistic failure probability predictions and resilience to withstand that shock.[4]

$$P_f\,(E<0)=\left(\sum\nolimits_{i=1}^{n}E_i\le 0\right) \tag{28}$$

where P_f is the probability of failure, and E_i is the energy dissipation at *i*th case.

In the conservative approach to structural analysis, the spring action of concrete is typically excluded. Instead, the focus is placed on the most frequent and extreme condition cases, as represented by the limiting equations (Eqs. (29) and (30)). LSEs estimated without considering the concrete contribution as spring action and recoiling are illustrated by Eqs. (29) and (30).

$$E_1=614.41+86.94*\frac{\gamma}{\eta}+3.32*\frac{10^5}{t^2}-0.5*M_{veh}*V_{max}^2 \tag{29}$$

$$E_2=3195.81+86.94*\frac{\gamma}{\eta}+1.72*\frac{10^6}{t^2}-4.2*10^4 \tag{30}$$

where E, γ/n, k_{col}, M_{veh}, and V_{max}, t represent energy dissipated, a ratio controlling post-impact energy dissipation,

column stiffness, vehicle weight, maximum colliding speed, and impact duration in milliseconds.

Considering concrete contribution as spring action

During a vehicle impact, concrete behaves like a nonlinear spring, initially resisting deformation with increasing stiffness via spring action. As the load intensifies, micro-cracking reduces its stiffness, absorbing energy before potential failure. The contributions of spring action within the context of the LSE (likely referring to a "Load-Displacement System" or similar model) are thoroughly examined using the energy concept. In this context, spring action refers to the force exerted by the spring in response to compression or extension, typically governed by Hooke's law. The energy concept, in turn, helps quantify the potential energy stored in the spring, which can be critical for understanding the system's mechanical behavior, such as in structural analysis, elasticity, or dynamic response.

By incorporating the energy concept, the system models how energy is transferred, stored, or dissipated as the spring undergoes deformation. The potential energy stored in the spring is usually expressed as $0.5 * k_{col} * \Delta^2$, where k_{col} is the spring constant in terms of pier stiffness, and Δ represents displacement. This allows for a deeper analysis of the spring's behavior across different conditions, offering insights into how it contributes to the overall system dynamics.

$$E_3 = 614.41 + 86.94 * \frac{\gamma}{n} + 0.5 * k_{col} * \Delta^2 + 3.32 * \frac{10^5}{t^2} - 0.5 * M_{veh} * V_{max}^2 \quad (31)$$

$$E_4 = 3195.81 + 86.94 * \frac{\gamma}{n} + 0.5 * k_{col} * \Delta^2 + 1.72 * \frac{10^6}{t^2} - 4.2 * 10^4 \quad (32)$$

where E, γ/n, k_{col}, M_{veh}, V_{max}, and Δ represent energy dissipated, a ratio controlling post impact energy dissipation, column stiffness, vehicle weight, maximum colliding speed, and displacement, respectively.

The behavior of the spring is captured mathematically in two key scenarios:

- Eq. (31) represents the most common or typical case, corresponding to situations where the spring operates under standard, expected conditions. In this case, the spring's response is likely linear, meaning the force is directly proportional to the displacement. This scenario typically involves moderate forces and displacements, where the system is stable and predictable. The energy considerations here are straightforward, focusing on the elastic behavior of the spring without significant deviations.
- Eq. (32), on the other hand, represents the extreme or limiting case. This refers to conditions where the spring is subjected to high stress, large displacements, or nonlinear behavior. In these extreme scenarios, the spring may approach or exceed its elastic limit, potentially leading to permanent deformation or failure. The energy considerations here are more complex, as they may involve nonlinear force–displacement relationships, hysteresis, or damping effects. This case is crucial for understanding how the system behaves under high stress or near-failure conditions.

The LSE is then solved using the generated variables by using the RAND function via EXCEL. This process is repeated many times using randomly generated uniformly distributed variables. The probability of failure (P_f) is then estimated by dividing the number of times the LSE simulation is less than 0 by the total number of simulations (N) carried out. The β can be directly computed from P_f as shown in Eqs. (24) and (25).[29,30]

$$P_f = \frac{n}{N} \quad (33)$$

$$\beta = -\Phi^{-1}(P_f) \quad (34)$$

where n is the number of times the limit state has been exceeded ($g(x) < 0$), N is the total number of simulations undertaken, P_f is the probability of failure, β represents reliability index, and Φ^{-1} is the inverse of the standard normal cumulative distribution function (CDF).

MC simulation was employed due to its robust ability to analyze the effects of uncertainty and variability within mathematical models and real-world systems. By conducting numerous iterations with randomly generated inputs, MC enables a comprehensive exploration of potential outcomes. In this study, four identical scenarios were simulated using 11,000 iterations each, an amount determined adequate as the results had begun to converge beyond this point. The outcomes of these simulations are illustrated in Figs. 6–9.

Risk assessment using confidence interval (CI)

In this present study, the confidence interval (CI) is very significant to be determined. CI is defined as the degree of uncertainty for assessing the numerical results evaluated from dynamic simulation using the normal distribution. CI is also able to evaluate the probability that a parameter falls between a pair of values around the mean by addition and subtraction. Thus, the CI is utilized to assess uncertainty using the mean (μ), standard deviation (SD), confidence level (z), and sample size (N) (as shown in Table 1), as shown in Eq. (35).[27,28]

$$CI = \mu \pm z.\frac{SD}{\sqrt{N}} \quad (35)$$

where μ is the mean of the sample size, SD is the standard deviation, N is the sample size considered as 1000 data points, and z is the confidence or significance level considered as 98%.

The data used to capture and quantify the uncertainty were obtained from Figs. 6 through 9. The CI has been determined from Eq. (35) and is detailed in Table 1. This table provides a comprehensive overview of the various parameters and their associated uncertainties, offering valuable insights into the reliability and precision of the results. By analyzing these values, we can better understand the range of possible outcomes and assess the degree of confidence in the findings.

Uncertainty assessment

In structural impact and its post-impact behavior, understanding and managing uncertainty is crucial for ensuring the safety and resilience of structures exposed to dynamic loads such as collisions, explosions, or earthquakes. These impacts often introduce variables that are difficult to predict, including material properties, load characteristics, and potential measurement errors. Uncertainty investigation helps engineers assess and quantify these variables, enabling more reliable designs and risk assessments. These have been determined through characterizing structural serviceability and resilience, comprising the limit state, particularly by virtue of energy dissipation (E_i for i = 1, 2, 3, and 4), and need an insightful investigation before their widespread implementation and incorporation into the design. To estimate LSE scrupulously, uncertainty ($\bar{U}_E$) investigation based on the parametric results (R), considering independent variables as x_1, x_2, x_3, …, x_n, becomes an indispensable task for mitigating risk factors. Thus, the general formulation to estimate R is as shown in Eq. (36).[29]

$$R = R(x_1, x_2, x_3, \ldots\ldots\ldots\ldots\ldots, x_n) \tag{36}$$

The overall uncertainty due to energy dissipation ($\bar{U}_E$) can be determined by normalizing the respective uncertainties resulting from Eq. (37), as shown in reference.[28] The overall uncertainty in the result is given by carrying out the partial derivative, as shown in Eq. (37).[29]

$$\bar{U}_E = \pm\left[\left(\frac{\partial\bar{U}}{\partial\bar{U}_{E1}}.\bar{U}_{E1}\right)^2+\left(\frac{\partial\bar{U}}{\partial\bar{U}_{E2}}.\bar{U}_{E2}\right)^2+\left(\frac{\partial\bar{U}}{\partial\bar{U}_{E3}}.\bar{U}_{E3}\right)^2+\left(\frac{\partial\bar{U}}{\partial\bar{U}_{E4}}.\bar{U}_{E4}\right)^2\right]^{1/2} \tag{37}$$

where $\bar{U}_{E1}$, $\bar{U}_{E2}$, $\bar{U}_{E3}$, and $\bar{U}_{E4}$ are the respective uncertainties in the independent variables.

Results

Using MC simulations

Energy dissipation at specific damage scenario

When a high-velocity truck collides with a RC column, the truck's kinetic energy is rapidly dissipated through a combination of material and structural mechanisms. The impact induces high strain rates, leading to concrete cracking, crushing, and fragmentation, as well as yielding and possible strain hardening of the steel reinforcement. Bond-slip between steel and concrete further contributes to energy dissipation. Structurally, the column may undergo flexural and shear deformations, potentially form plastic hinges, or experience brittle shear failure, depending on the impact location and column detailing. Additional energy is absorbed through localized damage at the impact zone, such as punching shear or penetration, and some energy is dispersed as vibrations and elastic waves. The extent and mode of energy dissipation are influenced by the impact velocity, column geometry, reinforcement configuration, and boundary conditions.

Energy dissipation in a specific high-velocity impact damage scenario occurs through complex mechanisms such as concrete spalling, micro-cracking, crushing, and friction within the concrete matrix. These processes convert kinetic energy from the impact into irreversible material deformation, reducing the overall force transmitted. Results are captured using the corresponding LSE to ensure safety and serviceability by extracting energy dissipation. It also defines the boundary between acceptable and unacceptable performance of a structure's viability and resilience under given loads. This is shown below through Figs. 7 and 8.

Case I: Without Concrete Contribution.

Case II: Considering concrete contribution as spring or recoiling action.

The values of failure probability (P_f) derived from Figs. 7 and 8 are 0.0001 and 0.00012, respectively. These results indicate a minimal contribution from the concrete in resisting dynamic loads from trucks or semi-trailers, particularly in

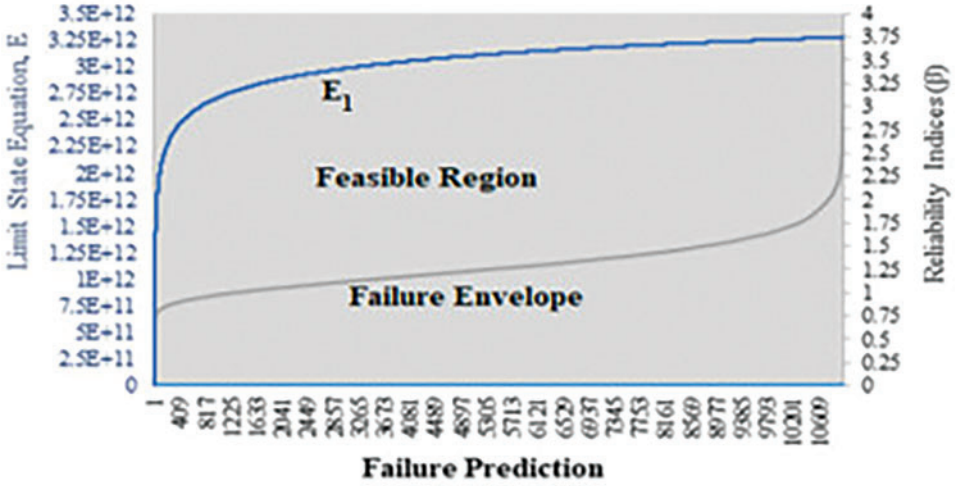

Figure 7. Results without spring action not frequently occurring

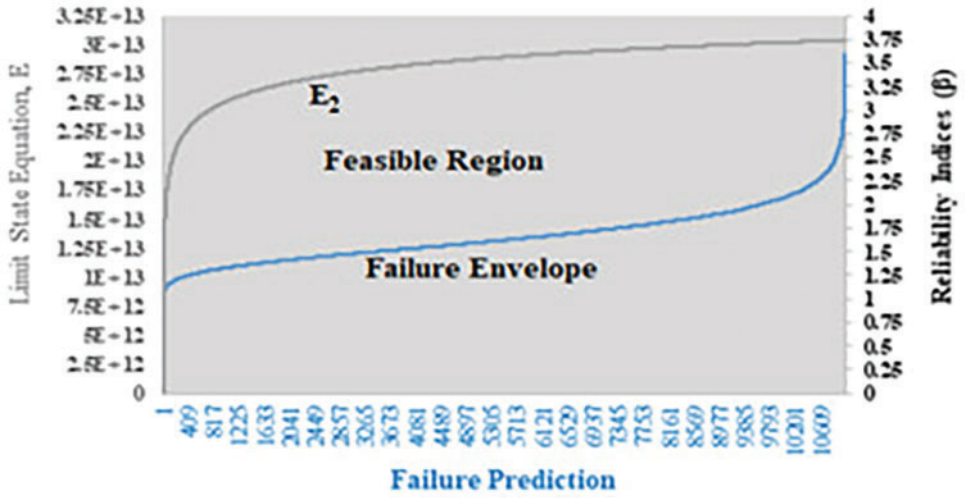

Figure 8. Results without spring action, most frequently occurring

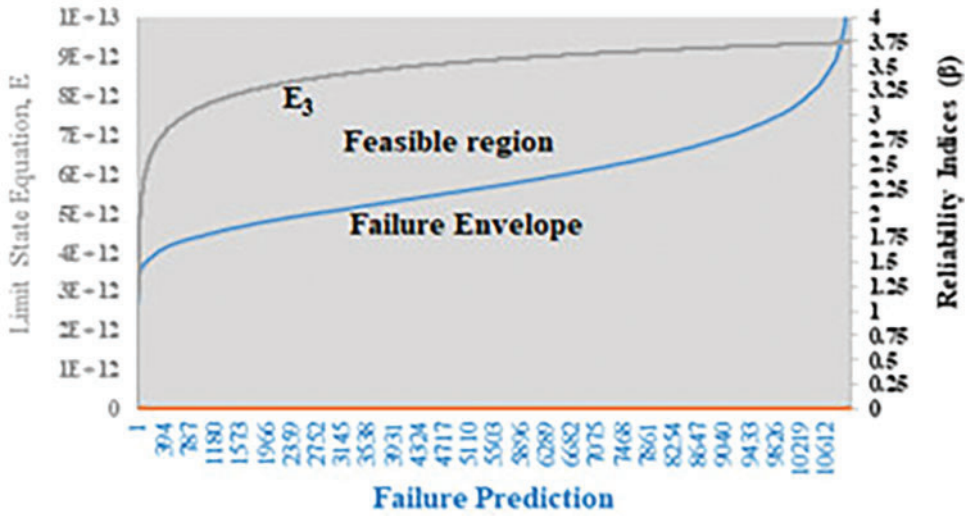

Figure 9. Results with spring action for most frequently occurring

Table 1. Input data for to estimate CI

Input variables	M (in-kip)	Z	SD (in-kip)	N	CI (in-kip)
E_1	5713	0.5	5712	1000	5713 ± 31.62
E_2	5713	0.5	5712	1000	5713 ± 31.62
E_3	5896	0.5	5895	1000	5896 ± 93.21
E_4	6121	0.5	6120	1000	6121 ± 96.77

terms of recoil action. In contrast, Figs. 9 and 10 depict concrete as being modeled to contribute through both recoiling and elastic (spring-like) behavior, yielding significantly lower failure probabilities of 0.00005 and 0.000056. This highlights the impact of modeling assumptions on structural response under localized failure scenarios.

A conservative approach, which neglects any elastic contribution from the concrete (i.e., assumes no spring action), results in lower values of the structural response modifier β. Although this method provides a higher margin of safety, it leads to more optimistic predictions of system reliability, as it underestimates the structure's capacity to absorb and dissipate energy. Conversely, when concrete's spring action is considered—acknowledging its capacity to resist deformation and contribute to energy dissipation—the resulting β values are significantly higher. This reflects a system with greater resilience and improved resistance to localized failure, as supported by prior findings.[23]

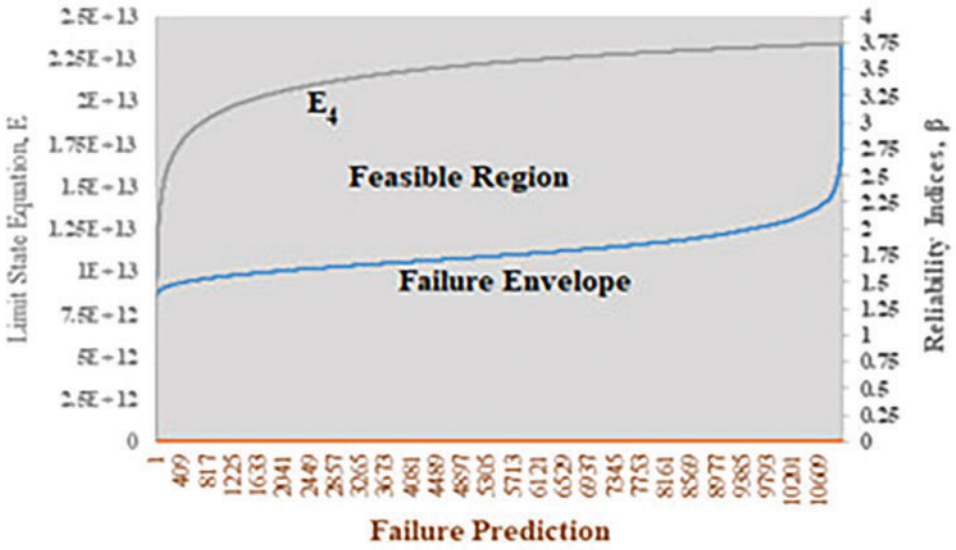

Figure 10. Results with spring action for most conservatively occurring

Specifically, energy dissipation domains derived from Figs. 7 and 8 show that β ranges from $2.25 \leq \beta \leq 4.1$, corresponding to P_f in the range of 10^{-4} to 10^{-5}. Conservative modeling (Figs. 7 and 9) confines the reliable design region to $2.25 \leq \beta \leq 3.75$, where failure is less likely. On the other hand, when the concrete's spring-like behavior is integrated (Figs. 8 and 10), a broader and higher reliability domain is obtained, with β ranging from $2.25 \leq \beta \leq 3.75$.

Furthermore, in Fig. 11, various energy values (E) are normalized against the most favorable corresponding β values. This plotting facilitates the identification of optimal β–E relationships, establishing a comprehensive understanding of how energy absorption capability scales with structural robustness. These relationships serve as a basis for more accurate failure predictions and improved performance-based design strategies.

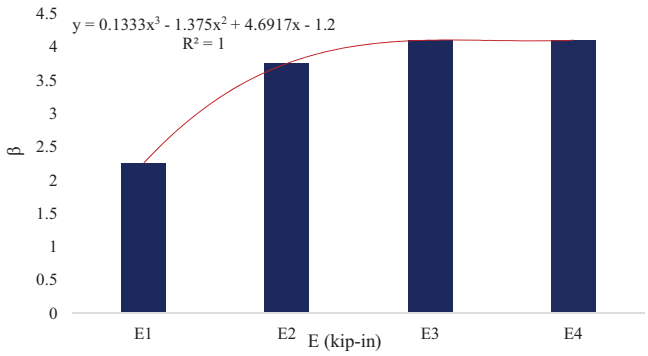

Figure 11. Obtaining β from various E

From Fig. 11, a good trade-off between β and various E values is obtained, as shown in Eq. (38), which provides a steady relationship.

$$\beta = 0.133 * E^3 - 1.375 * E^2 + 4.692 * E - 1.2 \quad (38)$$

where β and E have already been explained.

Using CI

The CI, utilizing key statistical parameters, serves as a critical tool for examining energy dissipation criteria, as illustrated in Table 1. By calculating the CI, we can quantify the degree of uncertainty around energy measurements, providing insight into how reliable the observed data are when making inferences about energy dissipation. This is particularly useful when the measurements are subject to variability or measurement errors, ensuring that we can assess the range within which the true values likely lie. To fully leverage this approach, a deeper analysis is necessary, especially in terms of understanding how the CI can be applied to energy dissipation patterns over time or across different conditions.

Specifically, the relationship between E+ and E−, as detailed in Table 1, plays a pivotal role in this analysis. These two metrics represent energy values under different conditions, E+ could be indicative of energy dissipated under certain parameters, while E− may reflect a contrasting scenario. By comparing these values, we can gain a better understanding of how energy dissipation behaves in different environments or systems.

This relationship has been graphically represented in Fig. 11, where the correlation between E+ and E− is visualized. Such a visualization not only clarifies the nature of the relationship between these two forms of energy but also helps to illustrate trends, such as how changes in one might influence the other. Furthermore, the graph offers a means of visually interpreting the statistical results from Table 1, allowing for a more intuitive grasp of the data. The visualization enhances our understanding of the underlying phenomena associated with energy dissipation, providing a clear, empirical basis for examining the effectiveness and efficiency of energy usage in various systems. Through this combined use of statistical intervals and graphical representation, the significance and reliability of the findings from the present study can be better assessed.

In Fig. 12, the estimated CI for the corresponding E_+ and E− has been plotted with respective R^2 values of 0.98

and 0.99, representing two degrees of polynomial equations. These are captured from Fig. 12 and shown in Eqs. (39) and (40), respectively.

$$CI^{+} = 57.14 * E_{+}^{2} - 119.3 * E_{+} + 5793.70 \quad (39)$$

$$CI^{-} = 55.36 * E_{-}^{2} - 161.80 * E_{-} + 5786.80 \quad (40)$$

where CI^{+} and CI^{-} represent the positive and negative values of the CI using Table 1, and E_{+} and E− address the positive and negative values of energies dissipated.

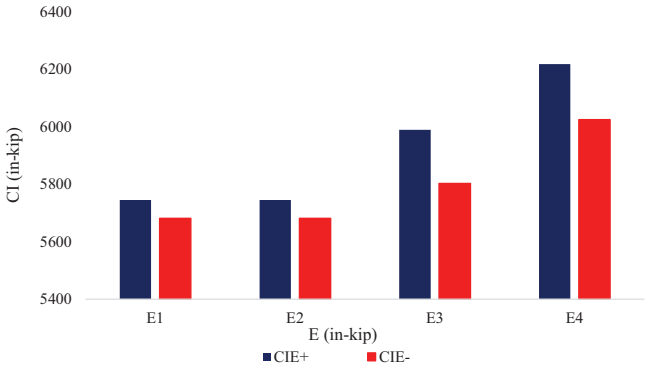

Figure 12. CI for corresponding E+ and E−

Eqs. (39) and (40) are derived through the systematic normalization of the energy-based formulations previously defined in Eqs. (29) to (32). This normalization process serves two critical purposes. First, it transforms the original equations into dimensionless forms, allowing for a more generalized analysis that is not constrained by specific units or scales. Second, and more importantly, it facilitates the identification and exclusion of parameters that exert minimal influence on the system's energy dissipation behavior.

During normalization, dimensionless groups are formed by comparing characteristic quantities such as material stiffness, damping, loading rate, and deformation scales. Parameters that consistently exhibit negligible contributions across a wide range of scenarios, such as certain geometric tolerances, secondary inertial terms, or minor damping factors, are systematically discarded. This simplification does not compromise the accuracy of the model but rather strengthens it by concentrating on the principal drivers of the dissipation mechanism, such as strain energy in concrete, contact friction, and dynamic interaction between structural components.

As a result, Eqs. (39) and (40) emerge as refined expressions that retain the dominant terms governing energy dissipation during impact or localized failure. These equations are not only easier to interpret and compute but also more physically meaningful. They provide clearer insight into the relationship between structural behavior (e.g., stiffness, resistance to failure) and energy absorption mechanisms under dynamic loads, such as those imposed by heavy vehicles or other transient forces.

By adopting this approach, the analysis achieves a higher level of abstraction while maintaining fidelity to the underlying mechanics. This makes Eqs. (39) and (40) particularly useful for parametric studies, design optimization, and failure prediction in performance-based engineering frameworks.[24,25]

The statement describes a model for the post-impact behavior of a pier, where the energy response (E) is normalized regardless of the type of energy dissipation involved. It considers both positive (E_{+}) and negative (E_{-}) energy responses, developing a generalized relationship with a parameter (β) that influences the behavior. This relationship is holistic, meaning it accounts for various factors and conditions, and is illustrated in Fig. 13, showing how normalized E and β are interrelated in the context of the pier's behavior after impact.

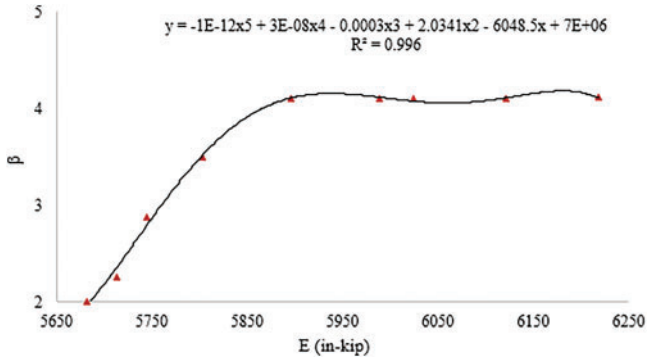

Figure 13. β from corresponding E where β and E have already been addressed

Fig. 13 helps to capture a holistic relationship between β and E, and can be precisely determined from Eq. (41).

$$\beta = -10^{-12} * E^{5} + 3 * 10^{-8} * E^{4} - 0.0003 * E^{3} + 2.034 * E^{2} - 6048.50 * E + 7 * 10^{6} \quad (41)$$

The model, comprising a fifth-degree polynomial with a tight R^2 value of 0.996, presents a normalized energy response (E) of a pier post-impact, considering both positive (E+) and negative (E−) energy states, and independent of dissipation type. It establishes a generalized relationship with the parameter (β), as shown in Fig. 13.

Using uncertainty

Uncertainty analysis in vehicle impact energy dissipation involves systematically identifying and quantifying the various sources of uncertainty that influence how accurately we can estimate the amount of kinetic energy absorbed or lost when a vehicle collides with a structure, such as a bridge pier. These uncertainties arise from multiple factors, including variability in material properties (like concrete strength and steel ductility), differences in vehicle speed, impact angle, structural geometry, and modeling assumptions used in simulations or experiments. By propagating these uncertainties through analytical methods, the range of possible outcomes and the confidence level of their predictions regarding structural response and damage can be precisely predicted. This process is crucial because it helps ensure that safety assessments and design decisions for impact-resistant structures are robust, accounting for the inherent variability and incomplete knowledge present in real-world scenarios.

Ultimately, uncertainty analysis enhances the reliability of impact energy dissipation estimates, guiding more effective design and mitigation strategies to protect infrastructure and save lives.

During a vehicle impact, kinetic energy is rapidly transferred and dissipated through the vehicle structure and the material it collides with—often concrete in the form of barriers, walls, or road surfaces. In such scenarios, energy dissipation plays a critical role in mitigating damage and injury. When a vehicle crashes into concrete, the metal components of the vehicle undergo significant deformation, particularly in designed crumple zones, which absorb and redistribute energy away from occupants. Concrete, being a brittle and non-ductile material, behaves differently—it resists initial deformation due to its high compressive strength but fractures suddenly under high tensile stress. Upon impact, concrete dissipates energy primarily through cracking, fragmentation, and internal microcracking, which propagate radially from the point of contact. Unlike ductile materials that deform plastically and absorb energy gradually, concrete exhibits a sharp loss of structural integrity once its tensile threshold is exceeded, releasing stored elastic energy through crack propagation. Additionally, part of the kinetic energy is transferred into vibrations and heat, contributing to overall energy dissipation. The horizontal spread of these forces within both the vehicle and the concrete structure is critical in understanding how the collision energy is managed, and it informs the design of safer vehicles and more resilient RC bridge piers.

Uncertainty plays a crucial role in predicting energy dissipation. Factors such as material variability and imperfect surface contact make it challenging to precisely quantify energy loss in real-world collisions. Consequently, uncertainty can affect the accuracy of energy conservation models, necessitating probabilistic approaches to account for variations in material behavior and external influences. This study presents the energy dissipation (E) and associated uncertainties for various cases as shown in Fig. 13.

From the plotted Fig. 14, the estimated $\bar{U}_{Ei}$ for the corresponding E_i has been plotted with tight R^2 values of 1.0, representing third-degree polynomial equations. This has been captured from Fig. 12 and is shown in Eqs. (42).

$$\overline{U}_{Ei} = 0.02 * E_i^3 - 0.21 * E_i^2 + 0.46 * E_i + 3.84 \quad (42)$$

where $\bar{U}_{Ei}$ represents the percent uncertainty for the respective E_i, where i = 1, 2, 3, and 4.

However, using Eq. (37) and via Eq. (42), the estimation of overall $\bar{U}$ yields a trivial deviation of ±8%.

Generalized LSE

The generalized Limit State Equation (LSE) technique has been refined through the normalization and linearization of key variables, specifically the parameters E, CI, and $\bar{U}_{Ei}$. This refinement is achieved by performing a thorough data analysis using regression methods. The core objective of this approach is to adjust and control the parameter β, which plays a crucial role in governing energy dissipation during high-strain-rate vehicle impacts.

These impacts, typically marked by rapid deformation, lead to complex energy behaviors driven by the intense strain-rate load generated in high-velocity vehicle crashes. By utilizing regression techniques, the model effectively captures the nuances of energy dissipation, providing a more accurate understanding of how energy is transferred and lost during such high-impact events.

This enhanced methodology offers deeper insights into the dynamics of vehicle crashes, significantly improving the accuracy and reliability of energy dissipation models under extreme conditions. As a result, it contributes to better predictive capabilities and more robust analyses of energy behavior during high-speed collisions.

The final estimation of LSE used to precisely determine β is given by Eq. (43), which provides an optimal estimate by minimizing the sum of squared residuals between the observed and predicted values.[26]

$$\beta = -0.95 * E_i + 0.38 * \overline{U}_{Ei} - 898 * CI \quad (43)$$

where β, E_i, $\bar{U}_{Ei}$, and CI have already been explained.

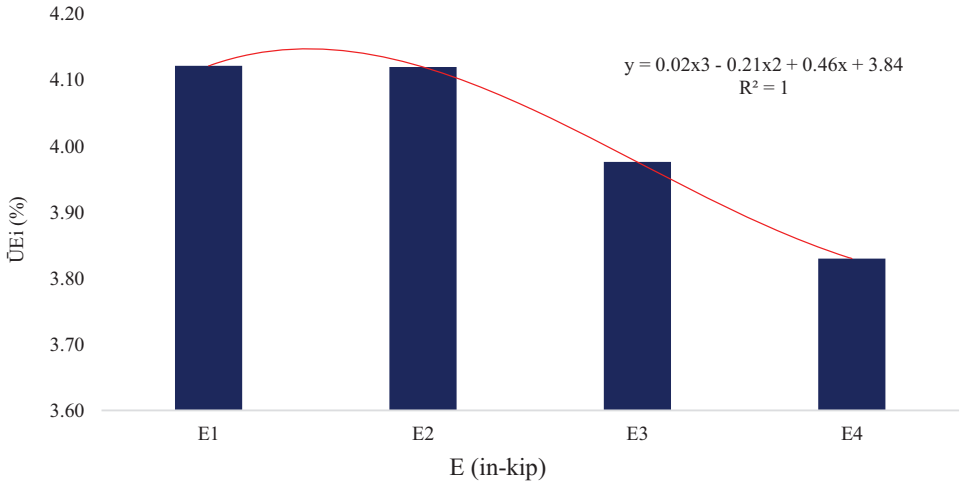

Figure 14. U_E^i for corresponding E_i

This is further addressed by complying with dependent variables β and $\bar{U}_{Ei}$ in terms of the dependent variable E, as shown in Fig. 15.

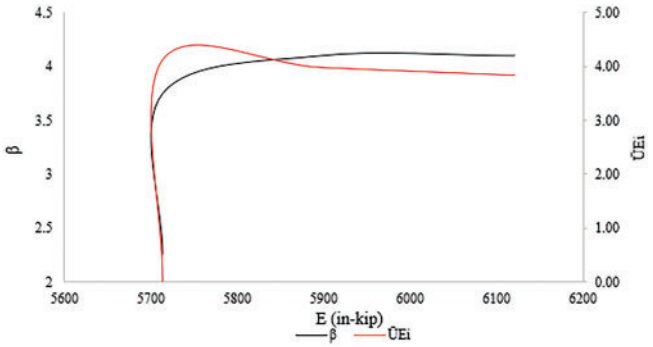

Figure 15. β and $\bar{U}_{Ei}$ observations from E_i

Discussion and Analysis of Results

In RC bridge structures, piers are particularly vulnerable to high-velocity vehicle collisions due to their exposed positions, yet current design standards lack clear performance criteria for such impacts. This study addresses the urgent need to evaluate and mitigate the susceptibility of RC piers by focusing on crack initiation as a critical indicator of energy dissipation during short-duration, high-impact events. By employing advanced analytical methods combined with extensive MC simulations, the research offers a deeper understanding of material behavior, inter-material interactions, and dynamic structural responses, ultimately providing essential insights to improve resilience and prevent catastrophic failure under collision scenarios.

From the simulation results, an LSE framework has been developed to reliably assess structural performance under impact. The outcome of the LSE is subjected to rigorous validation through multiple checks, which lead to CIs and uncertainty evaluations. A holistic, normalized version of the LSE was derived using multivariate regression and subsequent data analysis, allowing for more accurate reliability predictions based on various input parameters.

While the developed approach shows promise, further studies are required before it can be widely applied in practice. Based on the comparative analysis of the simulation results, the following conclusions can be drawn:

i) This study investigates various dynamic impact scenarios by examining concrete's inherent resilience, particularly its spring-like action and its influence on post-impact behavior. A detailed assessment of energy dissipation mechanisms is conducted to quantify damage to bridge piers, focusing on the critical time frame of 10^{-3} to 10^{-4} s during which material behavior shifts from quasi-static to plastic deformation. Simultaneously, steel strain rates are mathematically modeled to capture the complex energy dissipation processes under high-velocity vehicle impacts. The total energy dissipation, along with the energy dissipated specifically by the embedded reinforcing steel bars due to time-dependent variation under high-velocity impact, has been quantified and is illustrated in Figs. 4 and 5. Utilizing a MC simulation approach, the analysis explores a range of load and strain effects (LSEs), with results expressed through the inverse CDF, $\Phi^{-1}(Pi)$, effectively depicting strain rate evolution across the quasi-static to plastic regimes. These findings, illustrated in Figs. 6–9, provide a robust framework for understanding and predicting concrete durability and resilience under dynamic impact conditions.

ii) The prediction of normalized reliability within the model, as defined by Eq. (10), is calculated by estimating the reliability index β, which incorporates the energy dissipation parameter E under various conditions. This approach enables a reliable evaluation of pier performance through a normalized measure of energy dissipation, highlighting the critical role played by the sacrificial layer and pier cover in mitigating damage. The energy dissipation process is closely linked to concrete cracking and, in some cases, spalling, providing an indirect but effective means of assessing pier integrity. This relationship between β and normalized energy dissipation is formalized in Eq. (38) and visually represented in Fig. 11, offering valuable insight into how damage mechanisms influence overall structural reliability.

iii) The determination of CI, together with the corresponding dissipated energy from high-velocity vehicle impacts, establishes an improved relationship that enriches the understanding of the dynamic interplay among key response parameters. This integrated framework clarifies the interconnection between the CI, reliability index β, and normalized energy dissipation (E), thereby enabling a more precise modeling of post-impact behavior in structural systems. By capturing these relationships, the analysis advances the predictive capability for assessing damage and resilience under dynamic impact conditions.

iv) Figures 13–15, the energy dissipation trends for both positive (E+) and negative (E−) values, when utilizing CI, follow a similar pattern, with polynomial equations showing a close fit (R^2 values of 0.98 and 0.99). Although there is a gradual increase in the percent difference between E+ and E−, rising from 1.1% to 3.3%, this deviation remains small and does not significantly impact the overall model. The minimal increase in energy dissipation difference further demonstrates the robustness and accuracy of the model, confirming its ability to reliably represent the energy dissipation behavior for both E+ and E−, corroborating energy dissipation followed by post-damage severity, overall reliability, and specific impact withstanding ability.

v) A comprehensive investigation into the model's uncertainty was undertaken by first quantifying the

individual uncertainties associated with various components, followed by their aggregation to evaluate the overall impact. These uncertainties were normalized and graphically represented in Fig. 13, facilitating a clearer and more consistent comparison by removing the effects of differing scales and units. Subsequent regression analysis of the normalized uncertainties revealed a third-degree polynomial relationship with an R^2 value of 1.0, indicating an exact fit between the model and the observed data. This outcome underscores the model's robustness, demonstrating that even with an uncertainty margin of ±8%, it consistently delivers highly accurate predictions, thereby confirming its reliability and practical applicability in real-world structural impact scenarios.

vi) Eq. 42 has been rigorously developed using multivariate regression analysis to produce a comprehensive and reliable model that integrates key variables such as Ei, the CI, and $\bar{U}i$, while systematically addressing inherent uncertainties and variabilities. This robust formulation for the reliability index β effectively accounts for the complex interplay of factors influencing structural response. To further elucidate the normalized energy dissipation (E) as a post-impact phenomenon, Fig. 14 presents a graphical depiction capturing the holistic relationships among E, β, and $\bar{U}i$. This visualization clarifies the interdependencies among these variables, thereby deepening the understanding of their combined influence and enhancing the precision of the model's predictive capabilities.

vii) In essence, this article presents a comprehensive investigation into predicting energy dissipation in RC bridge piers subjected to high-velocity vehicular impacts. By integrating MC (MC) simulations with a rigorously developed and normalized limit state (LS) model, the study evaluates the reliability of the structural system under dynamic loading. The research intricately explores the complex behavior of concrete as the primary energy-absorbing material, detailing how it manages short-duration impact loads through sophisticated mechanisms. Central to this work is the formulation of limit state equations (LSEs) that effectively quantify energy dissipation while rigorously incorporating model uncertainties. This holistic approach enables a robust assessment of the model's applicability to real-world conditions. Among the key findings, strong correlations are identified between energy dissipation (E), reliability index (β), and normalized variables ($\bar{U}i$), providing valuable insight into the dynamic performance and resilience of RC bridge piers under extreme impact scenarios.

Conclusions and Future Work

This study presents a detailed simulation-based investigation into the failure behavior of a RC bridge pier subjected to vehicular impact, with a specific emphasis on understanding energy dissipation mechanisms. The pier is impacted at a height of 3 ft above its base, representing a realistic collision scenario involving standard vehicle bumpers. To capture a range of possible outcomes, multiple impact scenarios are modeled, varying parameters such as vehicle speed, mass, and angle of impact. These simulations evaluate the pier's structural resistance and the evolution of damage under dynamic loading. A key component of the analysis is the implementation of lumped spring elements (LSE), which allow for a simplified yet effective representation of energy absorption and redistribution within the system. By modeling the post-impact response through LSE, the study captures the interactions between the vehicle and the pier, including the transfer of kinetic energy, material deformation, and localized failures. The findings offer valuable insights into how RC piers dissipate energy during impact events, supporting the development of more resilient design strategies and improved predictive models for dynamic structural performance under various short-duration, high strain-rate loading conditions.

The analysis contrasts two approaches: conservative and nonconservative, by assessing the concrete's role in energy dissipation and its ability to resist failure. In the conservative approach, the concrete contribution is neglected, while in the nonconservative approach, concrete is modeled as providing spring-like action, which enhances energy dissipation and reduces the load transferred to the steel reinforcement. This spring-like action not only helps in absorbing impact energy but also reduces the stress on the steel, which can lead to a more efficient design by minimizing steel requirements.

In furtherance of this study, the nonconservative approach contributes to the pier's ability to avoid catastrophic collapse during an impact, thus improving the residual capacity of the structure. The geometry of the pier, including its aspect ratio, plays a critical role in its performance under impact, influencing its capacity to absorb and dissipate energy effectively. Overall, these factors highlight the importance of considering both material behavior and structural geometry when designing RC piers for impact resilience.

To determine the amount of energy dissipation responsible for plastic deformation, γ/η plays a significant role. Failure followed by plastic hinge formation due to impact is only possible if the entire dissipated energy has been governed by the steel bar in the ranges of quasi-static to plastic strain within the 10^{-3} to 10^{-4} second time domain. As an extension of this research, it is recommended that further studies include the structure for a more realistic design and reliability. It is recommended that the following are incorporated into future studies:

i) Combinations of different grades of concrete with different steel grades at various strain rates should be investigated for quasi-static and dynamic loads.

ii) Nonlinear analysis has been undertaken in this research to study the crack propagation at different strain rates. However, nonlinear analysis at static conditions is highly recommended to calibrate β_T. A more conservative and comprehensive value is recommended to extend the boundaries for precisely

predicting the dynamic behavior of post-impacted materials' interactive behavior during the application of high strain rate loading.

iii) In this study, the maximum permissible crack-width limit has been considered from the ACI crack limit at moisture. However, different crack widths in different exposures, weather conditions, different geometries, and various types of vehicle impact scenarios demand improved reliability analysis to ascertain the ability to withstand necessary impact loads from high-velocity car crash scenarios.

iv) Due to their geometry and exposed faces, the vulnerability of RC bridge piers to high-velocity impact in terms of crack propagation has been thoroughly investigated. This will help to provide a meticulous understanding for estimating optimum resilience in post-impact scenarios. Various geometries along with different impact scenarios are recommended to be carried out before reaching decisions. This will help provide explicit insights into possible crack determination and collapse, to determine crack resistance methodologies.

v) Furthermore, the study highlights the urgent need to update and calibrate existing design codes to more accurately capture the complex load–resistance interactions observed in real-world impact scenarios. These proposed refinements seek to enhance structural design standards, ensuring that bridge piers are better prepared to withstand the intensified forces generated by high-velocity vehicular impacts. By integrating the research findings, engineers can significantly improve the resilience and safety of critical infrastructure, enabling bridge piers to more effectively absorb and dissipate energy during extreme impact events. Ultimately, this leads to enhanced durability and performance, contributing to safer and more reliable transportation networks.

Table 2 provides a detailed conversion chart that serves as an essential reference for translating measurements between the US Customary Units and their corresponding International System of Units. Given that engineering and scientific disciplines often use both unit systems, this chart ensures seamless and accurate conversion of data, minimizing the risk of errors due to unit inconsistency. By standardizing these conversions, the chart supports clear communication and reliable comparison of results, which is especially important in this article where data from various sources and systems are integrated. Ultimately, it facilitates uniformity and precision in measurement reporting, enabling readers and practitioners to interpret and apply the information confidently across different unit frameworks.

Table 2. Conversion chart for the us customary to the equivalent SI units

US customary	SI unit
1 ksi	6.89 MPa (kN/mm^2)
1 psi	0.00689 Mpa (kN/mm^2)
1 kip-in.	0.113 kN-m
1 kip	4.45 kN
1 lbs	0.00445 kN
1 mph	1.61 km/h
1 ft-lb/s	0.00136 kN-m/s (1.36 N-m/s)

Declarations

I, Suman Roy, the corresponding author, declare that this manuscript is original in its content, has not been published before, and is not currently being considered for publication elsewhere.

Acknowledgments

Funding to support this research was provided by Utah State University, Logan, Utah, USA, through its Research and Innovative Technology Administration.

Competing Interests

The authors declare that there is no competing of interests.

Data Availability Statement

Some or all data, models, or code that support the findings of this study are available from the corresponding author upon reasonable request.

Funding

This research is funded by the Department of Civil and Environmental Engineering, Utah State University, Logan, UT, USA.

References

[1] ACI (American Concrete Institute). Recommendations for design of beam-column joints in monolithic reinforced concrete structures. 2011;73(7):375–393.

[2] Cao R, El-Tawil S, Agrawal AK, Xu X, Wong W. Behavior and design of bridge piers subjected to heavy truck collision. *J Bridg Eng*. 2019;24(7):04019057. doi:10.1061/(ASCE)BE.1943-5592.0001414.

[3] Engineers AS of C. *Minimum Design Loads for Buildings and Other Structures (ASCE/SEI 7–22)*. American Society of Civil Engineers; 2013.

[4] Nowak AS, Collins KR. *Reliability of Structures*. 2nd ed. CRC Press; 2012. doi:10.1201/b12913.

[5] Ayyub BM, McCuen RH. *Probability, Statistics, and Reliability for Engineers and Scientists*. 3rd ed. CRC Press; 2016. doi:10.1201/b12161.

[6] Dutta A, Mander JB. Capacity design and fatigue analysis of confined concrete columns. In: *Technical Report*. Buffalo,

NY: Multidisciplinary Center for Earthquake Engineering Research; 1998.
[7] ATC-40. Seismic Evaluation and Retrofit of Concrete Buildings, ATC-40 Report. Report, ATC-40; 1996.
[8] Pantelides CP, Ameli MJ, Parks JE, Brown DN. *Seismic Evaluation of Grouted Splice Sleeve Connections for Precast RC Bridge Piers in ABC*. Utah Department of Transportation; 2014. doi:10.15554/pcij.03012015.80.103.
[9] Sohel KMA, Al-Jabri K, Al Abri AHS. Behavior and design of reinforced concrete building columns subjected to low-velocity car impact. *Structures*. 2020;26(7):601–616. Elsevier. doi:10.1016/j.istruc.2020.04.054.
[10] Mirza SA. Flexural stiffness of rectangular reinforced concrete columns. *ACI Struct J*. 1990;87(4):425–435. doi:10.14359/3056.
[11] Zhao X, Wu Y-F, Leung AY, Lam HF. Plastic hinge length in reinforced concrete flexural members. *Procedia Eng*. 2011;14(11):1266–1274. doi:10.1016/j.proeng.2011.07.159.
[12] Sinha BP, Gerstle KH, Tulin LG. Stress-strain relations for concrete under cyclic loading. *J Proc*. 1964;61(2):195–212. doi:10.14359/7775.
[13] Kurama, Yahya C, Sri Sritharan, et al. Seismic-resistant precast concrete structures: State of the art. *Journal of Structural Engineering*. 2018;144(4):03118001. doi:10.1061/(ASCE)ST.1943-541X.0001972.
[14] Park H, Eom T. Energy dissipation capacity of flexure-dominated reinforced concrete members. In: *13th World Conference on Earthquake Engineering*. 2004:1–6. Vancouver, BC: Canada. doi:10.4203/ccp.75.111.
[15] Kowalsky MJ. Deformation limit states for circular reinforced concrete bridge columns. *J Struct Eng*. 2000;126(8):869–878. doi:10.1061/(asce)0733-9445(2000)126:8(869).
[16] Mander JB, Priestley MJ, Park R. Theoretical stress-strain model for confined concrete. *J Struct Eng (United States)*. 1988;114:1804–1826. doi:10.1061/(ASCE)0733-9445(1988)114:8(1804).
[17] Shi Y, Hao H, Li Z-X. Numerical derivation of pressure-impulse diagrams for prediction of RC column damage to blast loads. *Int J Impact Eng*. 2008;35(11):1213–1227. doi:10.1016/j.ijimpeng.2007.09.001.
[18] Tsang H, Lam NTK. Collapse of reinforced concrete column by vehicle impact. *Comput Civ Infrastruct Eng*. 2008;23: 427–436.
[19] Crawford JE, Holland TJ, Mendoza PJ, Murtha RN. A failure methodology based on shear deformation. In: *Recent Advances in Engineering Mechanics and their Impact on Civil Engineering Practice*. ASCE; 1983:985–988.
[20] Slawson TR. *Dynamic Shear Failure of Shallow-Buried Flat-Roofed Reinforced Concrete Structures Subjected to Blast Loading*. Army Engineer Waterways Experiment Station Vicksburg MS Structures Lab; 1984.
[21] Feyerabend M. *Hard Transverse Impacts on Steel Beams and Reinforced Concrete Beams*. Germany: University of Karlsruhe (TH); 1988.
[22] Initial stiffness of reinforced concrete columns and walls. World Conference on Earthquake Engineering; 2012; Lisbon, Portugal. ISBN: 978-1-63439-651-6.
[23] Li B. Initial stiffness of reinforced concrete columns and walls. World Conference on Earthquake Engineering; 2012; Lisbon, Portugal. ISBN: 978-1-63439-651-6
[24] Stewart MG. Reliability-based load factors for airblast and structural reliability of reinforced concrete columns for protective structures. *Struct Infrastruct Eng*. 2019;15(5):634–646. doi:10.1080/15732479.2019.1566389.
[25] Crosby D, Cheremisinoff NP. Practical statistics for engineers and scientists. *Technometrics*. 1988;30(2):234. doi:10.1080/00401706.1988.10488377.
[26] Holman JP. *Experimental Methods for Engineers*. 6th ed. McGraw-Hill; 1994. ISBN-10: 0070296669; ISBN-13: 978-0070296664.
[27] Roy S. *Sustainability and Resiliency Investigation of Grouted Coupler Embedded in RC ABC Bridge Pier at Vehicle Impact*. Journal of Engineering and Applied Sciences, and Science Publishing Group; 2024. doi:10.11648/j.eas.20240901.12. Date of publication: March 07, 2024.
[28] Roy S. Reliability, sustainability, resiliency, and performance investigation of an embedded splice-sleeve connector at high velocity semi-trailer impact. *Mechanical Engineering Advances*. 2024;2(2):1633. Academic Publishing Pvt. Ltd. doi:10.59400/mea.v2i2.1633.
[29] Roy S. Reliability analysis and uncertainty evaluation for assessing low velocity car impacted cosmetic damage of prototyped RC bridge pier. *Insight-Civil Engineering*. 2024;7(1):623. PiscoMed Publishing. doi:10.18282/ice.v7i1.623. Published on September 29, 2024.
[30] Nowak AS, Collins KR. *Reliability of Structures*. 2nd ed. CRC Press; 12 October 2012. doi:10.1201/b12913.
[31] Roy S, Sorensen A. Energy based model of vehicle impacted reinforced bridge piers accounting for concrete contribution to resilience. *International Probabilistic Workshop*; 2021; Cham: Springer International Publishing. pp. 301–315. doi:10.1007/978-3-030-73616-3_22.
[32] Roy Suman. Reliability, sustainability, resiliency, and performance investigation of an embedded splice-sleeve connector at high velocity semi-trailer impact. *Mech Eng Adv*. 2024;2(2):1633. doi:10.59400/mea.v2i2.1633.
[33] Roy S. Sustainability and resiliency investigation of grouted coupler embedded in RC ABC bridge pier at vehicle impact. *Eng Appl Sci*. 2024;9(1):14–33. doi:10.11648/j.eas.20240901.12.